IFNγ expression correlates with enhanced cytotoxicity in CD8$^+$ T cells

Varsha Pattu[2#], Elmar Kause[2], Hsin-Fang Chang[2], Jens Rettig[2], Xuemei Li[1,2*#]

[1] Department of Neurology, NHC Key Laboratory of Diagnosis and Treatment on Brain Functional Diseases, The First Affiliated Hospital of Chongqing Medical University, No.1 Youyi Road, Yuzhong District, Chongqing, 400016, China

[2] Cellular Neurophysiology, Center for Integrative Physiology and Molecular Medicine, (CIPMM), Saarland University, 66421 Homburg, Germany

[#] These authors contributed equally to this work and share first authorship

* Correspondence: 860941986@qq.com

Abstrat: CD8$^+$ T lymphocytes (CTLs) function as serial killers of infected or tumorigenic cells by secreting large quantities of interferon-gamma (IFNγ) and granzyme B (GzmB). IFNγ is a pleiotropic cytokine, its expression dynamics and precise role in CTL-mediated cytotoxicity remain incompletely understood. To investigate the relationship between IFNγ expression and CTL cytotoxicity, we analyzed IFNγ production, subcellular localization, cellular subtypes, degranulation capacity, and early activation markers in IFNγ-expressing CTLs. First, we found that IFNγ expression was rapid, transient, and required secondary T-cell receptor (TCR) stimulation, whereas GzmB was pre-stored in resting CTLs. Notably, two distinct IFNγ-expressing subsets, IFNγ^{hi} and IFNγ^{lo}, were identified, while only a single GzmB-expressing population was observed. Subsequently, we classified IFNγ-expressing CTLs into effector/effector memory (T_E/T_{EM}) and central memory (T_{CM}) subsets. IFNγ^{hi} cells exhibited a predominantly T_E/T_{EM} phenotype, whereas IFNγ^{lo} cells showed reduced effector characteristics and a higher proportion of T_{CM}. Next, degranulation assays revealed that IFNγ^{hi} CTLs displayed significantly higher surface expression of the lytic granule marker CD107a (33.75%) compared to IFNγ^{lo} CTLs (3.76%), despite comparable intracellular GzmB levels. This suggests that elevated IFNγ production correlates with CTL killing capacity. Further analysis demonstrated that IFNγ^{hi} CTLs exhibited extensive colocalization with

cis-Golgi and GzmB, indicating robust IFNγ synthesis and efficient sorting of mature IFNγ into cytotoxic granules (CGs) relative to IFNγ^{lo} CTLs. Finally, we compared IFNγ and CRTAM expression in naive versus activated CD8^{+} T cells upon TCR stimulation, demonstrating that transient CRTAM expression may critically regulate initial CTL activation and IFNγ production.

Introduction

CD8^{+} cytotoxic T lymphocytes (CTLs) are critical immune sentinels that protect the host against infections and malignancies. Upon antigen recognition by specialized antigen-presenting cells (APCs), naive CD8^{+} T cells (T_N) undergo clonal expansion and differentiate into short-lived effector CTLs (T_E), which migrate to peripheral tissues and inflammatory sites[1,2]. Most T_E undergo apoptosis during the contraction phase[3], while a small subset persists as long-lived memory T cells (T_M). These memory populations consist of at least two distinct subsets: central memory (T_{CM}) and effector memory (T_{EM}) T cells[4,5]. In mice, short-lived T_E downregulate L-selectin (CD62L) but retain partial expression of IL-7 receptor alpha (CD127)[6], whereas long-lived T_M constitutively express CD127. T_{CM} exhibit high CD62L expression, while T_{EM} downregulate CD62L. Notably, under chronic infections or cancer, persistent antigen exposure can drive naive T cells into a dysfunctional state termed T cell exhaustion (T_{EX})[7]. Understanding the heterogeneity and function of CTL substets is crucial to discern the complex dynamics of immune responses in various disease[8].

CTLs eliminate target cells through lytic (granzymes and perforin) and non-lytic (IFNγ and TNFα) mechanisms[9,10]. Their effector functions are regulated by transcription factors such as T-bet, Eomes, CRTAM (Class-I MHC-restricted T-cell associated molecule), T-box, and Runx family proteins[11–13]. The killing capacity of CTLs depends on cytotoxic granules (CGs) and degranulation efficiency[14]. CGs are secretory lysosomes (SGs) containing granzymes and perforin[15], enclosed by a lipid bilayer embedded with lysosome-associated membrane glycoproteins (LAMPs), including CD107a (LAMP-1), CD107b (LAMP-2), and CD63 (LAMP-3)[16]. Upon target recognition, CGs fuse with the plasma membrane, releasing their cytotoxic substances via exocytosis[13]. Since resting CTLs lack surface LAMPs, CD107a/b expression serves as a quantitative marker for degranulation[12].

Additionally, Fas ligand (FasL/CD95L), stored in specialized SGs, is externalized during degranulation to induce apoptosis in target cells[17]. Intriguingly, CTLs also express Fas receptor (Fas), enabling fratricidal killing (CTL-fratricide)—a mechanism that eliminates effector T cells during immune contraction[17].

Beyond direct cytotoxicity, CTLs exert effector functions via interferon-gamma (IFNγ) and tumor necrosis factor-alpha (TNFα) secretion. IFNγ is primarily produced by NK cells, Th1 cells, and $CD8^+$ T cells[18,19]. In murine models of *Mycobacterium tuberculosis* infection, $CD4^+$ and $CD8^+$ T cells are the dominant IFNγ producers in vivo[20]. IFNγ is a pleiotropic cytokine with dual roles—exhibiting antiviral[21,22] and antitumor activity while paradoxically promoting tumor progression in certain contexts[23–25]. Mechanistically, IFNγ signaling upregulates interferon regulatory factor-1 (IRF-1), which enhances MHC-I/II expression, rendering target cells more susceptible to CTL attack[26]. As a proinflammatory cytokine, IFNγ also activates macrophages to secrete TNFα and IL-6[27–29].

In this study, we investigated IFNγ production, subcellular localization, cellular subtypes, and cytotoxic function in IFNγ-expressing CTLs. We found that naive $CD8^+$ T cells rapidly acquire IFNγ production within 2 hours of TCR activation whereas GzmB expression is restricted to effector CTLs[30]. Activated CTLs exhibited transient, TCR-dependent IFNγ expression, contrasting with pre-stored GzmB in resting CTLs. Strikingly, $IFN\gamma^+$CTLs segregated into $IFN\gamma^{hi}$ and $IFN\gamma^{lo}$ subsets, while $GzmB^+$CTLs were homogeneous. $IFN\gamma^{hi}$ cells displayed a T_E/T_{EM} phenotype (low CD62L), whereas $IFN\gamma^{lo}$ cells resembled T_{CM} (high CD62L). Degranulation assays revealed that $IFN\gamma^{hi}$ CTLs exhibited significantly higher surface CD107a than $IFN\gamma^{lo}$ cells, suggesting superior lytic activity. Furthermore, $IFN\gamma^{hi}$ CTLs showed pronounced colocalization with cis-Golgi and $GzmB^+$ vesicles, reinforcing the link between IFNγ expression and cytotoxicity. Finally, comparative analysis of IFNγ and CRTAM expression in naive vs. activated $CD8^+$ T cells suggested that CRTAM may regulate early T cell activation and IFNγ production.

Results

Transient IFNγ expression depends on TCR re-activation in resting CTLs

To determine whether interferon-gamma (IFNγ) expression is constitutive or regulated in activated CTLs, we analyzed intracellular IFNγ dynamics following TCR re-stimulation as previous report[31]. Day 3–5 activated CTLs, with or without re-stimulation, were fixed, permeabilized (BD Cytofix/Cytoperm™), and stained for IFNγ-Alexa488 and GzmB-Alexa647 (without Golgi transport inhibition). Flow cytometry data were acquired and analyzed using FlowJo v10.

IFNγ- and GzmB- expressing CTLs was shown in pseudocolor plots in 4 h TCR re-stimulation (Figure 1A,B). In unstimulated CTLs, IFNγ was nearly undetectable, but its expression increased rapidly upon TCR re-stimulation (Figure 1A). Whereas large amount of GzmB exisited before restimulation and had less variation after TCR re-stimulation (Figure 1B). The expression level of IFNγ and GzmB in CTLs exhibited a maturation-dependent pattern and distinct kinetics. IFNγ expression (measured by MFI) showed a transient peak (Figure 1C), with day 5 CTLs displaying faster upregulation than day 3 CTLs at 2 h ($p = 0.020$), 3 h ($p = 0.004$), and 4 h ($p = 0.004$). Day 4 CTLs showed IFNγ MFI kinetics comparable to day 5 CTLs but significantly faster than day 3 at 3 h ($p = 0.044$). In contrast, GzmB MFI remained stable across day 3-5 CTLs during the 4-hour restimulation period (Figure 1D).

Longitudinal analysis revealed divergent temporal patterns: IFNγ levels peaked at 12 h before declining sharply by 24 h, while GzmB accumulated continuously. IFNγ MFI was significantly elevated at 6 h, 8 h, and 12 h compared to 24 h ($p = 0.021$, $p = 0.017$, and $p = 0.021$, respectively) (Figure 1E). Conversely, GzmB MFI showed progressive accumulation, with significantly higher levels at 24 h versus 4 h, 6 h, and 8 h ($p = 0.021$, $p = 0.037$, and $p = 0.039$), and at 12 h versus 4 h ($p = 0.042$) (Figure 1F).

In conclusion, in activated CTLs, the expression of IFNγ and GzmB exhibited a maturation-dependent pattern and distinct kinetics. IFNγ expression is transient, but GzmB expression lasts longger compared to IFNγ after TCR (re-)activation.

CTL subtype dynamics upon TCR re-stimulation

Cytotoxic T lymphocytes (CTLs) comprise distinct functional subsets, including effector cells (T_E), effector-memory cells (T_{EM}), and central-memory cells (T_{CM}). To determine whether IFNγ expression is subtype-specific and whether TCR re-stimulation alters the subtype composition of cultured CTLs, we stimulated activated CTLs with 10 μg/mL plate-bound anti-CD3e[31] for 0.5–4 h and analyzed subtype markers ($CD44^{hi}$ for T_E/T_{EM}, $CD62^{hi}$ for T_{CM}) by flow cytometry at multiple timepoints.

Neither the percentage of $CD44^+$ cells (Extended Data Figure 1A) nor CD44 MFI (Extended Data Figure 1B) changed significantly during 4 h re-stimulation, regardless of culture day (day 3–5), indicating that overall effector differentiation status of the culture remained stable, independent of TCR re-stimulation or culture duration. In contrast, $CD62L^+$ cell frequency (Extended Data Figure 1C) and CD62L MFI (Extended Data Figure 1D) declined sharply upon re-stimulation ($p < 0.05$), indicating a transition from T_{CM} to T_{EM} (Figure 2A–C).

Pseudocolor plots in quadrant (Figure 2A) revealed subtype distribution. Cells in Q1 (CD44+CD62-) were $T_{E/EM}$, Q2 (CD44+CD62+) were T_{CM}, Q3 (CD44-CD62+) were $T_{N.}$ Day 5 CTLs exhibited significantly more T_E/T_{EM} than day 3 CTLs at 4 h and day 4 CTLs at 1 h/4 h ($p < 0.05$; Figure 2B). Concurrently, T_{CM} frequency was lower in day 5 vs. day 3/day 4 CTLs at 1 h ($p < 0.05$; Figure 2C), confirming that longer culture promotes $T_{E/EM}$ differentiation upon re-stimulation.

Screening of activation markers (CD25, CD44, CD62L, CD69) in day 5 CTLs revealed robustly decreased CD62L and increased CD69 in both cell frequency and MFI (Figure 2D,E) after 2 h re-stimulation, while no significant changes were found in CD44 or CD25, implicating CD62L downregulation and CD69 upregulation are robust indicators of TCR-driven T_{CM}-to-T_{EM} transition.

Cellular subtype and cytotoxicity analysis of $IFN\gamma^{hi}$ and $IFN\gamma^{lo}$ CTLs

To determine whether IFNγ expression correlates with cytotoxic T lymphocyte (CTL) effector function, we analyzed reactivated CTLs, which exhibited distinct clusters of high ($IFN\gamma^{hi}$) and low ($IFN\gamma^{lo}$) IFNγ expression (Figure 1A and Figure 3A, row 1). Using a fluorescence intensity threshold of 10^3, we classified IFNγ-positive CTLs into $IFN\gamma^{hi}$ and $IFN\gamma^{lo}$ subsets (Figure 3A, row

2). Longed re-stimulation led to increased effector T cell (T_E) generation (Figure 2B & 3A row3). IFNγ^{hi} subset generated significantly higher ratio of T_E than IFNγ^{lo} subset at 3 and 4 hours of restimulation (Figure 3B).

Although IFNγ^{hi} and IFNγ^{lo} CTLs showed comparable CD44 expression, IFNγ^{hi} CTLs exhibited significantly lower CD62L levels compared to IFNγ^{lo} CTLs (Supplement 2). The proportion of T_{CM} was slightly higher in IFNγ^{lo} CTLs, though not statistically significant (Figure 3C). When assessing IFNγ production kinetics, IFNγ^{hi} CTLs displayed markedly higher IFNγ MFI than IFNγ^{lo} CTLs at 2, 3, and 4 hours post-stimulation (Figure 3D), whereas GzmB MFI did not differ significantly between the two subsets (Figure 3E).

Extended TCR stimulation revealed a pronounced divergence in IFNγ fluorescence between IFNγ^{hi} and IFNγ^{lo} CTLs by 24 hours (p = 0.001), while GzmB fluorescence remained comparable (Extended Data Figure 3). In IFNγ^{hi} CTLs, IFNγ fluorescence peaked at 12 hours before declining significantly by 24 hours (vs. 4 h, p = 0.042 and p = 0.0025). In contrast, IFNγ^{lo} CTLs exhibited a gradual increase, peaking at 12 hours without subsequent decline, and showed higher fluorescence at 6, 12, and 24 hours than at 4 hours (p = 0.0483, p = 0.0112, and p = 0.0063, Extended Data Figure 3A). GzmB fluorescence in IFNγ^{hi} CTLs rose significantly at 6, 8, and 24 hours (vs. 4 h, p = 0.0022, p = 0.0075, and p = 0.0213), whereas in IFNγ^{lo} CTLs showed increased GzmB only at 12 and 24 hours (vs. 4 h, p = 0.0246 and p = 0.0171, Extended Data Figure 3B).

To evaluate cytotoxic capacity, we measured CD107a surface expression, a marker of degranulation. Unstimulated CTLs exhibited minimal CD107a expression (~5%), but upon 3-hour re-stimulation, levels surged to 21.33% (day 3) and 57% (day 5), with day 5 showing significantly higher degranulation than day 3 (p = 0.0109; Figure 3F), suggesting that degranulation capacity escalates with CTL maturation. Notably, IFNγ^{hi} CTLs consistently displayed higher CD107a expression than IFNγ^{lo} CTLs (Figure 3G). Flow cytometry histograms depicted CD107a fluorescence intensity in unlabeled (gray), IFNγ^{hi} (pink), and IFNγ^{lo} (blue) CTLs (Figures 3Gi and 3Giii). On day 3, 33.75% of IFNγ^{hi} CTLs underwent degranulation versus only 3.76% of IFNγ^{lo} CTLs (Figure 3Gii). By day 5, degranulation frequencies rose to 75.47% (IFNγ^{hi}) and 31.13% (IFNγ^{lo}) (Figure 3Giv). These results suggests that cytotoxic activity correlates positively with IFNγ expression and cellular maturation, underscoring the functional superiority of IFNγ^{hi} CTLs.

Subcellular localization analysis of IFNγ in IFNγ^{hi} and IFNγ^{lo} CTLs

To characterize the spatial distribution of IFNγ in cytotoxic T lymphocytes (CTLs), we analyzed the Pearson's correlation coefficient (PCC) between endogenous IFNγ, cis-Golgi, and granzyme B (GzmB) in IFNγ^{hi} and IFNγ^{lo} subsets.

IFNγ colocalized with the Golgi Apparatus. Wild-type (WT) CTLs were re-stimulated with plate-bound aCD3e and stained for endogenous IFNγ and cis-Golgi. Super-resolution structured illumination microscopy (SIM) was performed using ZEN software, and PCC was quantified with Fiji. IFNγ exhibited extensive colocalization with cis-Golgi in WT CTLs. No significant difference in IFNγ-Golgi PCC was observed between IFNγ^{hi} and IFNγ^{lo} CTLs at 2 hours post-stimulation on day 4 (Figure 4A, B), while significantly higher colocalization in IFNγ^{hi} CTLs was displayed than IFNγ^{lo} CTLs after 4 hours of re-stimulation on day 2 (Figure 4C, D).

IFNγ localized in cytotoxic granules (CGs). To determine whether IFNγ traffics to CGs, we analyzed IFNγ and GzmB colocalization in GzmB-mTFP knock-in (KI) CTLs on days 2 and 5 post-stimulation. GzmB is a marker for CGs. SIM imaging (Figure 4E, F) and Fiji-based quantification (Figure 4G, H) revealed that a subset of IFNγ localized in GzmB+ CGs, with IFNγ^{hi} CTLs exhibiting significantly greater IFNγ-GzmB association than IFNγ^{lo} CTLs (Figure 4F, H).

Comparative localization in Golgi vs. CGs. IFNγ showed robust cis-Golgi localization in GzmB-mTFP KI CTLs, with IFNγ^{hi} CTLs displaying higher enrichment than IFNγ^{lo} CTLs (Figure 4F, H). In contrast, GzmB exhibited minimal Golgi association, though IFNγ^{hi} CTLs on day 5 demonstrated slightly higher GzmB-Golgi PCC than IFNγ^{lo} CTLs (Figure 4H). No such difference was observed on day 2 (Figure 4F).

These findings demonstrate that: The IFNγ^{hi} subset retains higher IFNγ expression and greater IFNγ localization within CGs compared to IFNγ^{lo} CTLs. Newly synthesized IFNγ accumulates more prominently in the Golgi apparatus than GzmB following acute TCR stimulation. The preferential trafficking of IFNγ to CGs in IFNγ^{hi} CTLs suggests a direct role in cytotoxicity, consistent with their enhanced effector function. IFNγ expression is dynamically regulated, with transient Golgi-associated production preceding effector granule loading. Together, these data support a model wherein IFNγ^{hi} CTLs achieve superior cytotoxic activity through coordinated IFNγ synthesis, Golgi processing, and granule loading.

Temporal regulation of CRTAM and IFNγ in naive and activated CTLs

To investigate the relationship between activation markers and IFNγ expression during early and late T cell activation, we analyzed IFNγ, CRTAM, CD62L, CD69, and CD25 expression in wild-type $CD8^+$ T cells at day 0 (naive) and day 5 (activated) following TCR stimulation or restimulation.

Kinetics of CRTAM and IFNγ expression. Both CRTAM and IFNγ were upregulated upon TCR stimulation (Figure 5A-F, Extended Figure 4A-C). $CRTAM^+$CTLs increased from 5.93% (1 h) to a peak of 96.6% (24 h) before declining to 10.4% by 72 h, while $IFN\gamma^+$CTLs rose from 5.24% (1 h) to 35.6% (24 h) and subsequently decreased to 9.62% (72 h) (Extended Figure 4B). Median fluorescence intensity (MFI) for both molecules peaked at 24 h and became nearly undetectable by 72 h (Extended Figure 4C). Notably, day 2 and day 3 CTLs regained CRTAM and IFNγ expression upon restimulation (4 h and 3 h, respectively), confirming their transient, activation-dependent regulation (Extended Figure 4A).

Comparative expression of CRTAM and IFNγ in naive vs. activated CTLs. Day 5 CTLs exhibited significantly higher percentage of $IFN\gamma^+$CTLs and IFNγ MFI than day 0 CTLs (Figure 5A-C), whereas naive CTLs had a greater proportion of $CRTAM^+$CTLs (Figure 5D,E). CRTAM MFI, however, did not differ significantly between day 0 and day 5 (Figure 5F). Quadrant analysis of pseudocolor plots revealed distinct coexpression patterns.

In day 0 CTLs, only 20–25% of $CRTAM^+$CTLs expressed IFNγ, but nearly 100% of $IFN\gamma^+$CTLs were $CRTAM^+$ after 14 h stimulation (Figure 5G, I; Extended Figure 4A). In day 5 CTLs, ~71% of $IFN\gamma^+$CTLs coexpressed CRTAM (Figure 5H, I).

Naive $IFN\gamma^+$CTLs also displayed higher CRTAM MFI than their day 5 counterparts (Figure 5J). Strikingly, $CRTAM^{hi}$ CTLs produced more IFNγ than $CRTAM^{lo}$ subsets (Figure 5K, L), underscoring a positive correlation between CRTAM and IFNγ.

Activation marker dynamics. CRTAM upregulation in naive CTLs occurred as rapidly as CD69 induction, preceding CD25 expression (1–6 h; Extended Figure 4A,D,G). Conversely, CD62L levels declined post-stimulation (Extended Figure 4J). By day 2, CTLs entered contraction/memory phases, marked by rising CD62L and declining CD69/CD25 (Extended Figure 4E,F,I,L). With TCR

restimulation, day2/3 CTLs were marked with reducing CD62L and increasing CD69/CD25 (Extended Figure 4E,F,H,I,L), while the percentage of CD25 didn't change (Extended Figure 4K).

Our findings demonstrate that CRTAM and IFNγ are transiently expressed in a TCR-dependent manner. CRTAM serves as an early activation marker and correlates with IFNγ production in naive CTLs. CRTAM, CD62L, CD69, and CD25 collectively define CTLs' activation states. These results position CRTAM as a key early responder during primary CTLs' activation, functionally linked to IFNγ-mediated effector responses.

Discussion

Effector $CD8^+$ T cells (CTLs) are central to antimicrobial and antitumor immunity, employing both lytic and non-lytic cytotoxic mechanisms. While their lytic function mediated by granzyme B (GzmB) and perforin is well-characterized[30,32], the role of interferon-gamma (IFNγ) in CTL-mediated cytotoxicity remains less defined. Our study elucidates the dynamic expression profile of IFNγ in activated CTLs and its functional contribution to their cytotoxic potential.

IFNγ dynamics and cytotoxic function. We demonstrate that IFNγ expression in CTLs is rapidly induced upon TCR activation, peaking early before declining transiently compared to the sustained expression of GzmB (Figure 1A–G). This transient expression coincided with CTL maturation, as evidenced by the progressive shift toward effector T cell (T_E) phenotypes and the downregulation of CD62L (Figure 2). Notably, CTLs segregated into distinct $IFN\gamma^{hi}$ and $IFN\gamma^{lo}$ subsets, with the former exhibiting a stronger effector phenotype (Figure 3A–C).

Intriguingly, $IFN\gamma^{hi}$ CTLs displayed significantly enhanced degranulation capacity (Figure 3D,G) despite comparable GzmB levels to $IFN\gamma^{lo}$ CTLs (Figure 3E), suggesting that IFNγ potentiates lytic cytotoxicity independently of intracellular GzmB expression level. This was further supported by super-resolution imaging, which revealed greater colocalization of IFNγ with GzmB-positive cytotoxic granules in $IFN\gamma^{hi}$ CTLs (Figure 4E–H). These findings position IFNγ not only as an immunomodulatory cytokine but also as a direct contributor to the lytic efficiency of CTLs. This finding is aligned with our previous research demonstrating that lytic IFNγ is stored within GzmB-containing cytotoxic granules and co-secreted at the immune synapse by effector $CD8^+$ T cells, a mechanism that enhances cytotoxic T lymphocytes' (CTLs) killing capacity[33]. Bhat et al.

(2017) demonstrated that autocrine IFNγ production by CTLs enhances their motility and facilitates killing of primary target keratinocytes, both in vitro and in vivo. This finding highlights the critical dependence of $CD8^+$ T cell cytotoxic function on local IFNγ signaling, which has important implications for immunotherapy targeting chronic viral infections and cancers[34].

CRTAM as a regulator of early CTL activation. The mechanisms governing IFNγ production in CTLs remain incompletely understood. Our data highlight CRTAM (class-I MHC-restricted T-cell-associated molecule) as a key early activation marker that correlates with IFNγ expression. CRTAM was upregulated transiently in naive CTLs upon TCR stimulation, preceding IFNγ induction (Figure 5; Extended Data Figure 3). Nearly all $IFN\gamma^+$CTLs coexpressed CRTAM during primary activation (Extended Data Figure 3A), and $CRTAM^{hi}$ subsets produced significantly more IFNγ than $CRTAM^{lo}$ cells (Figure 5K,L).

CRTAM's role in CTL biology aligns with its known functions in promoting IFNγ production in $CD8^+$ T cells and $CD4^+$ T cells[35,36], in regulating $CD4^+$ T cell polarization and in determing $CD4^+$ cytotoxic T lymphocyte lineage[35,37]. Its interaction with CADM1 may facilitate early CTL priming by retaining activated cells in lymphoid tissues[11], while its decline in day 5 CTLs (Figure 5I,J) suggests a stage-specific role in bridging early activation with effector differentiation.

Future directions. While our work establishes a link between IFNγ expression and CTL cytotoxicity, the molecular pathways connecting CRTAM to IFNγ regulation warrant further investigation. Single-cell RNA sequencing could delineate the transcriptional programs distinguishing $IFN\gamma^{hi}$ and $IFN\gamma^{lo}$ subsets[38–40], offering insights into their functional specialization. Additionally, mechanistic studies are needed to clarify whether IFNγ enhances lytic function through granule trafficking and fusion, target cell sensitization, or other effector pathways.

Conclusion. Our findings redefine IFNγ as a dual-function cytokine in CTLs, contributing to both immunomodulation and lytic cytotoxicity. The identification of CRTAM as an early regulator of IFNγ production underscores the complexity of CTL activation and provides a framework for future studies aimed at optimizing T cell-based therapies against infections and cancers.

Methods

Mice

Wild-type (WT) mice were purchased from Charles River , and granzyme b-mTFP knock-in (GzmB-mTFP KI) mice were generated as previously described[30].

Cell isolation

Mice were anesthetized with CO_2 and executed by cervical dislocation. The left abdominal cavity was exposed, and the spleen was carefully removed, placed on a 70 μm cell strainer (Corning Life Sciences) and ground. The grinding slurry remaining on the strainer was rinsed with RPMI medium, and the cell suspension (10 mL) was collected into a 15 mL sterile centrifuge tube (Corning Life Sciences) and centrifuged (6 min, 1100 rpm without a break) to wash the splenocytes. Washed splenocytes were mixed and incubated with erythrocyte lysis buffer (1 mL) for 30 seconds to lyse the erythrocytes therein. Immediately, 10 mL of ice-cold RPMI was added to terminate lysis and centrifuged (6 min, 1100 rpm), and the cell sediment was washed once more with isolation buffer to remove erythrocyte debris. Primary $CD8^+$ T lymphocytes were positively isolated from spleens according to the instructions of the Dynabeads FlowComp Mouse CD8 Kit (Thermo Scientific).

Cell culture

Isolated primary $CD8^+$ T lymphocytes were cultured at a density of 1×10^6 cells/mL in AIM V medium (Gibco) supplemented with 10% FCS, 50 μM β-Mercaptoethanol (BME), and 100 U/mL recombinant mouse IL-2 (Life technology) and stimulated with anti-CD3e/anti-CD28 magnetic beads (number of cells: magnetic beads = 1:0.8, Thermo Fisher Scientific) to generate activated CTLs. Cells were cultured in 24-well plates in a cell culture incubator (37 °C, 5% CO_2, saturated humidity) according to the protocol of Bzeih et al. (2016)[41]. The first passaging of the cells was started after 2 days of culture and then once a day with the addition of fresh AIM V medium supplemented with 10% FCS, 50 μM BME and 100 U/mL recombinant IL-2. Usually, day3 to day5 cells were used for experiments.

For some experiments, cells were used immediately after the CD3e/CD28 activation beads had been

removed. For most experiments cells were allowed to recover for 2 h after CD28/CD3e beads had been removed. Those cells underwent a “re-stimulation” during the experiment. By this is meant that by appropriate measures, the T-lymphocyte receptors have been acutely stimulated to trigger cytotoxic actions, such as the release of GzmB and IFNγ. For FACS experiments: To induce intracellular IFNγ-expression, day3-5 beads-activated WT CTLs were washed and restimulated with optimal concentration of plate-bound anti-CD3e antibody (10 µg/mL) from Estl et al. (2020)[29] for 0, 0.5 h, 1 h, 2 h, 3 h, and 4 h, 6 h, 8 h, 12 h and 24 h in a cell culture incubator.

Immunocytochemistry

CTLs were stained with an anti-IFNγ antibody to detect endogenous IFNγ. Therefore, cells were fixed with freshly prepared ice-cold 4% paraformaldehyde in DPBS (1×) and washed in DPBS (1×) containing 0.1 M glycine (quenching of autofluorescence). After a second wash cells were permeabilized with for 20 minutes in DPBS (1×) containing 0.1% Triton-X 100 (Roth), then blocked for 20-30 minutes in blocking buffer contained 5% BSA. Finally, cells were stained with primary rat anti-mouse IFNγ (1:200) and secondary anti-rat antibodies (1:1000), or rat anti-mouse IFNγ-Alexa488 (1:200), before they were mounted and imaged using high-resolution structured illumination microscopy (SIM).

Antinodies used in this study were listed in Extended Data Table1.

Structure illumination microscopy

Structured illumination microscopy setup

The structured illumination setup (SIM) setup was from Zeiss (ELYRA PS.1). Images were acquired using a 63× Plan-Apochromat (NA1.4) objective with excitation light of 488, 561, and 647 nm and then processed for SIM to obtain higher resolutions. Z-stacks of 200 nm step size were used to scan cells. Zen 2012 software (Zen 2012; Carl Zeiss) was used for the acquisition and processing of the images for higher resolutions.

Colocalization analysis

For colocalization analysis the JACoP plugin (Bolte 2006) of Fiji (Johannes, 2012) was used.

Pearson's and Manders' overlap coefficients (Manders et al., 1993) were used for quantification of the degree of colocalization.

Flow cytometry

Intracellular IFNγ measurement

WT CTLs were washed with DPBS (1×) after restimulation for 0.5 h, 1 h, 2 h, 3 h, 4 h, 6 h, 8 h, 12 h, and 24 h with plate-bound anti-CD3e antibody (10 μg/mL). The pellet (0.5×10^6 CTLs) was resuspended in 250 μL fixation buffer and incubated on ice for 10 min using BD Cytofix/ Cytoperm™ Fixation/Permeabilization Kit (554714, BD Bioscience). Next, CTLs were centrifuged, resuspended in 100 μL wash buffer (1×) and stained for intracellular IFNγ and GzmB with rat anti-mouse IFNγ-Alexa488 (1:200) and rat anti-mouse GzmB-Alexa647 (1:200)) on ice (1 h). Cells were washed and measured by flow cytometry (FACS, BD FACSAria III). Data were analyzed using FlowJo v10.10.0_CL software (Celeza-Switzerland).

Surface markers analysis

$CD8^+$ T-lymphocytes either with or without (re)stimulation, were taken from cell culture and washed with cold-DPBS (1×). Next they were stained for CD62L, CD69 and CD25 using corresponding fluorescent Abs without fixation (live staining, 30 min on ice). Next, cells were washed twice with cold-wash buffer (1×) and resuspended in cold-DPBS (1×) for FACS analysis.

Degranulation assay

Activated WT CTLs were washed and resuspended in AIM V after removing beads from the culture. Cells (0.2×10^6/200 μL) were then cultured on a 10 μg/mL anti-CD3e coated or DPBS (1×) coated 96-well plate with 1 μL anti-CD107a-PE for 3 h at 37 °C for degranulation. The control cells were incubated without anti-CD107a-PE as a background signal. All cells were then washed twice with cold DPBS (1×) and checked by FACS. Data were analyzed using FlowJo software. Gates were set according to no fluorescence control cells. Each independent experiment had a duplicate.

Data analysis

For data analysis and to calculate the statistical significance, Fiji, ImageJ-win64, Microsoft Excel

(Microsoft), SigmaPlot 13 and GraphPad_Prism10.2.3 were used. The respective method to calculate statistical significance was given in the text for each figure. Figures were generated using FlowJo_v10.10.0_CL, GraphPad_Prism, Excel and PowerPoint.

Data availability

Additional data and information that support the findings of this study are available from the corresponding author upon reasonable request.

Acknowledgments

This work was supported by China Scholarship Council (CSC), grants from the Deutsche Forschungsgemeinschaft (SFB 894 to J. R. and V. P.), and the Postdoctoral Project Funding from the First Affiliated Hospital of Chongqing Medical University. We thank Anja Bergsträßer, Margarete Klose, Nicole Rothgerber and Katrin Sandmeier for excellent technical assistance.

Author Contributions

V.P. and X.L. conceived and designed the study. X.L. conducted flow cytometry experiments and performed data analysis. X.L. carried out structured illumination microscopy (SIM) imaging and completed co-localization analysis. J.R., V.P. and X.L. secured funding for the research. E.K. and H.-F.C. provided critical insights for data interpretation. E.K. and V.P. offered technical support for flow cytometry and structured illumination microscopy. X.L. drafted the manuscript with input from all authors. All authors reviewed, edited, and approved the final version of the manuscript.

Competing interests

The authors declare no competing interests.

References

[1] Weninger W, Manjunath N, von Andrian UH. Migration and differentiation of CD8+ T cells. *Immunol Rev*. 2002 Aug;186:221-33. doi: 10.1034/j.1600-065x.2002.18618.x. PMID: 12234374

[2] [2] Stemberger C, Huster KM, Koffler M, Anderl F, Schiemann M, Wagner H, Busch DH. A single naive CD8+ T cell precursor can develop into diverse effector and memory subsets. *Immunity*. 2007 Dec;27(6):985-97. doi: 10.1016/j.immuni.2007.10.012. PMID: 18082432

[3] Jameson SC, Masopust D. Diversity in T cell memory: an embarrassment of riches. *Immunity*. 2009 Dec 18;31(6):859-71. doi: 10.1016/j.immuni.2009.11.007. PMID: 20064446

[4] Sallusto F, Lenig D, Förster R, Lipp M, Lanzavecchia A. Two subsets of memory T lymphocytes with distinct homing potentials and effector functions. *Nature*. 1999 Oct 14;401(6754):708-12. doi: 10.1038/44385. PMID: 10537110

[5] Sallusto F, Geginat J, Lanzavecchia A. Central memory and effector memory T cell subsets: function, generation, and maintenance. *Annu Rev Immunol.* 2004;22:745-63. doi: 10.1146/annurev.immunol.22.012703.104702. PMID: 15032595

[6] Huster KM, Busch V, Schiemann M, Linkemann K, Kerksiek KM, Wagner H, Busch DH. Selective expression of IL-7 receptor on memory T cells identifies early CD40L-dependent generation of distinct CD8+ memory T cell subsets. *Proc Natl Acad Sci U S A.* 2004 Apr 13;101(15):5610-5. doi: 10.1073/pnas.0308054101. Epub 2004 Mar 25. PMID: 15044705

[7] Wherry EJ. T cell exhaustion. *Nat Immunol.* 2011 Jun;12(6):492-9. doi: 10.1038/ni.2035. PMID: 21739672.

[8] Koh CH, Lee S, Kwak M, Kim BS, Chung Y. CD8 T-cell subsets: heterogeneity, functions, and therapeutic potential. *Exp Mol Med.* 2023 Nov;55(11):2287-2299. doi: 10.1038/s12276-023-01105-x. Epub 2023 Nov 1. PMID: 37907738; PMCID: PMC10689838.

[9] Weigelin B, den Boer AT, Wagena E, Broen K, Dolstra H, de Boer RJ, Figdor CG, Textor J, Friedl P. Cytotoxic T cells are able to efficiently eliminate cancer cells by additive cytotoxicity. *Nat Commun.* 2021 Sep 1;12(1):5217. doi: 10.1038/s41467-021-25282-3. PMID: 34471116; PMCID: PMC8410835.

[10] Perdomo-Celis F, Taborda NA, Rugeles MT. CD8+ T-Cell Response to HIV Infection in the Era of Antiretroviral Therapy. *Front Immunol.* 2019 Aug 9;10:1896. doi: 10.3389/fimmu.2019.01896. PMID: 31447862

[11] Takeuchi A, Itoh Y, Takumi A, Ishihara C, Arase N, Yokosuka T, Koseki H, Yamasaki S, Takai Y, Miyoshi J, Ogasawara K, Saito T. CRTAM confers late-stage activation of CD8+ T cells to regulate retention within lymph node. *J Immunol.* 2009 Oct 1;183(7):4220-8. doi: 10.4049/jimmunol.0901248. Epub 2009 Sep 14. PMID: 19752223

[12] Cruz-Guilloty F, Pipkin ME, Djuretic IM, Levanon D, Lotem J, Lichtenheld MG, Groner Y, Rao A. Runx3 and T-box proteins cooperate to establish the transcriptional program of effector CTLs. *J Exp Med.* 2009 Jan 16;206(1):51-9. doi: 10.1084/jem.20081242. Epub 2009 Jan 12. PMID: 19139168

[13] Paley MA, Kroy DC, Odorizzi PM, Johnnidis JB, Dolfi DV, Barnett BE, Bikoff EK, Robertson EJ, Lauer GM, Reiner SL, Wherry EJ. Progenitor and terminal subsets of CD8+ T cells cooperate to contain chronic viral infection. *Science*. 2012 Nov 30;338(6111):1220-5. doi: 10.1126/science.1229620. PMID: 23197535

[14] Betts MR, Koup RA. Detection of T-cell degranulation: CD107a and b. *Methods Cell Biol.* 2004;75:497-512. doi: 10.1016/s0091-679x(04)75020-7. PMID: 15603439

[15] Peters PJ, Borst J, Oorschot V, Fukuda M, Krähenbühl O, Tschopp J, Slot JW, Geuze HJ. Cytotoxic T lymphocyte granules are secretory lysosomes, containing both perforin and granzymes. *J Exp Med.* 1991 May 1;173(5):1099-109. doi: 10.1084/jem.173.5.1099. PMID: 2022921

[16] Fukuda M. Lysosomal membrane glycoproteins. Structure, biosynthesis, and intracellular trafficking. *J Biol Chem.* 1991 Nov 15;266(32):21327-30. PMID: 1939168

[17] Bossi G, Griffiths GM. Degranulation plays an essential part in regulating cell surface expression of Fas ligand in T cells and natural killer cells. *Nat Med.* 1999 Jan;5(1):90-6. doi: 10.1038/4779. PMID: 9883845

[18] Kambayashi T, Assarsson E, Lukacher AE, Ljunggren HG, Jensen PE. Memory CD8+ T cells provide an early source of IFN-gamma. *J Immunol.* 2003 Mar 1;170(5):2399-408. doi: 10.4049/jimmunol.170.5.2399. PMID: 12594263

[19] Ivashkiv LB. IFNγ: signalling, epigenetics and roles in immunity, metabolism, disease and cancer immunotherapy. *Nat Rev Immunol.* 2018 Sep;18(9):545-558. doi: 10.1038/s41577-018-0029-z. PMID: 29921905

[20] Bold TD, Ernst JD. CD4+ T cell-dependent IFN-γ production by CD8+ effector T cells in Mycobacterium tuberculosis infection. *J Immunol.* 2012 Sep 1;189(5):2530-6. doi: 10.4049/jimmunol.1200994. Epub 2012 Jul 25. PMID: 22837486

[21] Costa-Pereira AP, Williams TM, Strobl B, Watling D, Briscoe J, Kerr IM. The antiviral response to gamma interferon. *J Virol.* 2002 Sep;76(18):9060-8. doi: 10.1128/jvi.76.18.9060-9068.2002. PMID: 12186889

[22] Rhein BA, Powers LS, Rogers K, Anantpadma M, Singh BK, Sakurai Y, Bair T, Miller-Hunt C, Sinn P, Davey RA, Monick MM, Maury W. Interferon-γ Inhibits Ebola Virus Infection. *PLoS Pathog.* 2015 Nov 12;11(11):e1005263. doi: 10.1371/journal.ppat.1005263. PMID: 26562011

[23] Gocher AM, Workman CJ, Vignali DAA. Interferon-γ: teammate or opponent in the tumour microenvironment? *Nat Rev Immunol.* 2022 Mar;22(3):158-172. doi: 10.1038/s41577-021-00566-3. Epub 2021 Jun 21. PMID: 34155388; PMCID: PMC8688586

[24] Mazet JM, Mahale JN, Tong O, Watson RA, Lechuga-Vieco AV, Pirgova G, Lau VWC, Attar M, Koneva LA, Sansom SN, Fairfax BP, Gérard A. IFNγ signaling in cytotoxic T cells restricts anti-tumor responses by inhibiting the maintenance and diversity of intra-tumoral stem-like T cells. *Nat Commun.* 2023 Jan 19;14(1):321. doi: 10.1038/s41467-023-35948-9. PMID: 36658158; PMCID: PMC9852295

[25] Jorgovanovic D, Song M, Wang L, Zhang Y. Roles of IFN-γ in tumor progression and regression: a review. *Biomark Res.* 2020 Sep 29;8:49. doi: 10.1186/s40364-020-00228-x.

PMID: 33005420

[26] Yang MQ, Du Q, Varley PR, Goswami J, Liang Z, Wang R, Li H, Stolz DB, Geller DA. Interferon regulatory factor 1 priming of tumour-derived exosomes enhances the antitumour immune response. *Br J Cancer.* 2018 Jan;118(1):62-71. doi: 10.1038/bjc.2017.389. Epub 2017 Nov 7. PMID: 29112686

[27] Karki R, Sharma BR, Tuladhar S, Williams EP, Zalduondo L, Samir P, Zheng M, Sundaram B, Banoth B, Malireddi RKS, Schreiner P, Neale G, Vogel P, Webby R, Jonsson CB, Kanneganti TD. Synergism of TNF-α and IFN-γ Triggers Inflammatory Cell Death, Tissue Damage, and Mortality in SARS-CoV-2 Infection and Cytokine Shock Syndromes. *Cell.* 2021 Jan 7;184(1):149-168.e17. doi: 10.1016/j.cell.2020.11.025. Epub 2020 Nov 19. PMID: 33278357

[28] Lochhead RB, Strle K, Arvikar SL, Weis JJ, Steere AC. Lyme arthritis: linking infection, inflammation and autoimmunity. *Nat Rev Rheumatol.* 2021 Aug;17(8):449-461. doi: 10.1038/s41584-021-00648-5. Epub 2021 Jul 5. PMID: 34226730

[29] Glass CK, Natoli G. Molecular control of activation and priming in macrophages. *Nat Immunol.* 2016 Jan;17(1):26-33. doi: 10.1038/ni.3306. PMID: 26681459

[30] Chitirala P, Chang HF, Martzloff P, Harenberg C, Ravichandran K, Abdulreda MH, Berggren PO, Krause E, Schirra C, Leinders-Zufall T, Benseler F, Brose N, Rettig J. Studying the biology of cytotoxic T lymphocytes in vivo with a fluorescent granzyme B-mTFP knock-in mouse. *Elife.* 2020 Jul 22;9:e58065. doi: 10.7554/eLife.58065. PMID: 32696761

[31] Estl M, Blatt P, Li X, Becherer U, Chang HF, Rettig J, Pattu V. Various Stages of Immune Synapse Formation Are Differently Dependent on the Strength of the TCR Stimulus. *Int J Mol Sci*. 2020 Apr 2;21(7):2475. doi: 10.3390/ijms21072475. PMID: 32252488

[32] Dustin ML, Long EO. Cytotoxic immunological synapses. *Immunol Rev.* 2010 May;235(1):24-34. doi: 10.1111/j.0105-2896.2010.00904.x. PMID: 20536553

[33] Li X, Schirra C, Wirkner ML, Tu SM, Lin CH, Hohmann M, Alawar N, Chouaib A, Becherer U, Pattu V, Rettig J, Krause E, Chang HF. Lytic IFNγ is stored in granzyme B-containing cytotoxic granules and co-secreted by effector $CD8^+$ T cells. *BioRxiv* 2025.01.29.635520; doi: https://doi.org/10.1101/2025.01.29.635520

[34] Bhat P, Leggatt G, Waterhouse N, Frazer IH. Interferon-γ derived from cytotoxic lymphocytes directly enhances their motility and cytotoxicity. *Cell Death Dis.* 2017 Jun 1;8(6):e2836. doi: 10.1038/cddis.2017.67. PMID: 28569770; PMCID: PMC5520949.

[35] Yeh JH, Sidhu SS, Chan AC. Regulation of a late phase of T cell polarity and effector functions by Crtam. *Cell*. 2008 Mar 7;132(5):846-59. doi: 10.1016/j.cell.2008.01.013. PMID: 18329370

[36] Boles KS, Barchet W, Diacovo T, Cella M, Colonna M. The tumor suppressor TSLC1/NECL-2 triggers NK-cell and CD8+ T-cell responses through the cell-surface receptor CRTAM. *Blood*. 2005 Aug 1;106(3):779-86. doi: 10.1182/blood-2005-02-0817. Epub 2005 Apr 5. PMID: 15811952

[37] Takeuchi A, Badr Mel S, Miyauchi K, Ishihara C, Onishi R, Guo Z, Sasaki Y, Ike H, Takumi A, Tsuji NM, Murakami Y, Katakai T, Kubo M, Saito T. CRTAM determines the CD4+ cytotoxic T lymphocyte lineage. *J Exp Med*. 2016 Jan 11;213(1):123-38. doi: 10.1084/jem.20150519.

Epub 2015 Dec 22. PMID: 26694968;

[38] Speiser DE, Wieckowski S, Gupta B, Iancu EM, Baumgaertner P, Baitsch L, Michielin O, Romero P, Rufer N. Single cell analysis reveals similar functional competence of dominant and nondominant CD8 T-cell clonotypes. *Proc Natl Acad Sci U S A*. 2011 Sep 13;108(37):15318-23. doi: 10.1073/pnas.1105419108. Epub 2011 Aug 29. PMID: 21876175

[39] Giles JR, Ngiow SF, Manne S, Baxter AE, Khan O, Wang P, Staupe R, Abdel-Hakeem MS, Huang H, Mathew D, Painter MM, Wu JE, Huang YJ, Goel RR, Yan PK, Karakousis GC, Xu X, Mitchell TC, Huang AC, Wherry EJ. Shared and distinct biological circuits in effector, memory and exhausted CD8+ T cells revealed by temporal single-cell transcriptomics and epigenetics. *Nat Immunol*. 2022 Nov;23(11):1600-1613. doi: 10.1038/s41590-022-01338-4. Epub 2022 Oct 21. PMID: 36271148

[40] Xue Z, Wu L, Tian R, Gao B, Zhao Y, He B, Sun D, Zhao B, Li Y, Zhu K, Wang L, Yao J, Liu W, Lu L. Integrative mapping of human CD8+ T cells in inflammation and cancer. *Nat Methods*. 2025 Feb;22(2):435-445. doi: 10.1038/s41592-024-02530-0. Epub 2024 Nov 29. PMID: 39614111.

[41] Bzeih H (2016) The Role of Synaptobrevin2 in Exo-Endocytosis in Primary Mouse Cytotoxic lymphocytes.

Figure Legends

Figure 1 | Intracellular IFNγ and granzyme B (GzmB) expression in activated CTLs. (A–D) WT CTLs (days 3–5 post-activation) were re-stimulated with plate-bound anti-CD3e antibody (10 μg/mL) and analyzed for intracellular IFNγ and GzmB expression over 0–4 h. **(A, B)** Pseudocolor plots depict fluorescence intensity of rat anti-mouse IFNγ-Alexa488 (x-axis) and GzmB-Alexa647 (x-axis) against side scatter area (SSC-A, y-axis). **(C, D)** Median fluorescence intensity (MFI) of IFNγ-Alexa488 and GzmB-Alexa647. **(E, F)** Temporal changes in IFNγ and GzmB expression in re-stimulated CTLs. MFI dynamics of IFNγ-Alexa488 and GzmB-Alexa647. Data are mean ± SEM ($N \geq 3$). Statistical significance was determined by one-way ANOVA and unpaired t-test (*$p < 0.05$, **$p < 0.01$, ***$p < 0.001$; NS, not significant).

Figure 2 | Surface activation marker expression profiles in CTLs analyzed by flow cytometry. (A–C) WT CTLs (days 3–5 post-activation) were re-stimulated with plate-bound anti-CD3e antibody (10 μg/mL) for 0–4 h and stained for CD44 and CD62L. **(A)** Pseudocolor plots depict fluorescence intensity of rat anti-mouse CD62L-APC (x-axis) and CD44-PE (y-axis). **(B, C)** Frequencies of T_E and T_{CM} populations. **(D, E)** WT CTLs (day 5 post-activation) were re-stimulated with plate-bound anti-CD3e (10 μg/mL) for 2 h and analyzed for multiple activation markers. **(D)** Fold change in CD44+, CD62L+, CD25+, and CD69+ cell populations. **(E)** MFI change of CD44-PE, CD62L-APC, CD25-PE, and CD69-APC before and after 2 h restimulation. Data represent mean ± SEM ($N \geq 3$). Statistical analysis was performed using one-way ANOVA and unpaired t-test (*$p < 0.05$, **$p < 0.01$, ***$p < 0.001$; NS, not significant).

Figure 3 | Characterization of IFNγ^{hi} and IFNγ^{lo} CTL subsets and their cytotoxic potential. (A-E) WT CTLs were re-stimulated with plate-bound anti-CD3e antibody for 0-4 h and processed for flow cytometry analysis: One aliquot was surface-stained with anti-CD44-APC and anti-CD62L-PE, followed by intracellular staining for IFNγ-Alexa488. Another aliquot was intracellularly stained for IFNγ-Alexa488 and GzmB-Alexa647 **(A)** Gating strategy and surface marker expression profiles of IFNγ^{hi} vs IFNγ^{lo} CTLs. **(B)** Percentage of effector T cells (T_E) in each subset. **(C)** Percentage of central memory T cells (T_{CM}) in each subset. **(D)** IFNγ fluorescence intensity in IFNγ^{hi} vs IFNγ^{lo} subsets. **(E)** GzmB fluorescence intensity in IFNγ^{hi} vs IFNγ^{lo} subsets.

(F,G) Degranulation capacity assessed by CD107a surface expression: Day 3 and 5 WT CTLs were stimulated with plate-bound anti-CD3e for 3 h in the presence of anti-CD107a-PE, followed by intracellular IFNγ staining. **(F)** Percentage of CD107a+ CTLs pre- and post-stimulation. **(G) i,iii**: CD107a expression in IFNγ^{hi} vs IFNγ^{lo} CTLs at day 3 and 5. **ii,iv**: CD107a fluorescence intensity in IFNγ^{hi} vs IFNγ^{lo} CTLs at day 3 and 5. Data represent mean ± SEM (N≥2 independent experiments). Statistical significance was determined by unpaired t-test (*p<0.05, **p<0.01, ***p<0.001).

Figure 4 | Subcellular localization of IFNγ in IFNγ^{hi} and IFNγ^{lo} CTL subsets. (A-H) WT or GzmB-mTFP KI CTLs were re-stimulated with plate-bound anti-CD3e (10 µg/mL) (for day2: 4 h restimulation, day4 and day 5: 2 h restimulation) and processed for super-resolution microscopy (SIM): Imaging and analysis: Cells were stained for IFNγ, GzmB, and cis-Golgi marker (GM130) IFNγ^{hi} vs IFNγ^{lo} subsets were imaged using optimized laser power and EMCCD gain settings. Colocalization analysis performed using Fiji-win64 software. Quantitative comparisons and graphing performed using GraphPad Prism 10.2.3. Experimental details: **(A-B)** Day 4 WT CTLs: Primary antibodies: Rat anti-mouse IFNγ-Alexa488 (1:200), mouse anti-GM130 (1:100). Secondary antibody: Goat anti-mouse-Alexa647 (1:1000). **(B)** Pearson's correlation coefficient for IFNγ and cis-Golgi colocalization. **(C-D)** Day 2 WT CTLs: Primary antibodies: Rat anti-mouse IFNγ (1:200), mouse anti-GM130 (1:100). Secondary antibodies: Alexa647 chicken anti-rat IgG (1:800), Alexa568 goat anti-mouse IgG (1:400). Imaging parameters: IFNγ^{lo}: 561 nm laser (1.5%, gain 80); 647 nm laser (1.5%, gain 50). IFNγ^{hi}: 561 nm laser (1.2%, gain 80); 647 nm laser (0.6%, gain 25). **(D)** Pearson's correlation coefficient analysis. **(E-H)** GzmB-mTFP KI CTLs: Primary antibodies: Rat anti-mouse IFNγ (1:200), mouse anti-GM130 (1:100). Secondary antibodies: Alexa647 chicken anti-rat IgG (1:800), Alexa568 goat anti-mouse IgG (1:400). **(E,F)** Day 2 CTLs imaging parameters: IFNγ^{hi}: 488 nm (22%, gain 80); 568 nm (1.2%, gain 80); 647 nm (0.7%, gain 40). IFNγ^{lo}: 488 nm (26%, gain 80); 568 nm (1.2%, gain 80); 647 nm (1.5%, gain 80). **(G,H)** Day 5 CTLs imaging parameters: IFNγ^{hi}: 488 nm (18%, gain 80); 561 nm (1.2%, gain 80); 647 nm (0.3%, gain 20). IFNγ^{lo}: 488 nm (16%, gain 80); 561 nm (1.5%, gain 80); 647 nm (1.0%, gain 80). **(F,H)** Pearson's correlation coefficient analyses. Statistical analysis: Data represent mean ± SEM. Significance was determined by one-way ANOVA with t-tests (*p<0.05, **p<0.01, ***p<0.001; NS, not significant).

Figure 5 | Co-expression analysis of CRTAM and IFNγ in activated CTLs by flow cytometry. Experimental design: Day 0 CTLs: Stimulated with plate-bound anti-CD3e (10 μg/mL) and anti-CD28 (5 μg/mL) for 14 h. Day 5 CTLs: Re-stimulated with plate-bound anti-CD3e (10 μg/mL) for 2 h in 96-well plates. Staining: Anti-CRTAM-PE and anti-IFNγ-Alexa488 antibodies. Flow cytometry analysis: **(A)** Representative pseudocolor plots of IFNγ expression in day 0 vs day 5 CTLs. **(B)** Frequency of IFNγ^{+}CTLs. **(C)** Median fluorescence intensity (MFI) of IFNγ-Alexa488. **(D)** Representative pseudocolor plots of CRTAM expression. **(E)** Frequency of CRTAM^{+}CTL populations. **(F)** MFI of CRTAM-PE. Co-expression analysis: **(G, H)** Quadrant plots showing IFNγ and CRTAM co-expression patterns. **(I)** Frequency of CRTAM^{+} cells in IFNγ^{+} CTLs. **(J)** MFI of CRTAM-PE in IFNγ^{+}CTLs. **(K-L)** MFI of IFNγ-Alexa488 in CRTAM^{hi} vs CRTAM^{lo} subsets. Statistical analysis: Data represent mean ± SEM (N=3 independent experiments). Significance was determined by unpaired t-test (*p<0.05, **p<0.01, ***p<0.001; NS, not significant).

Additional information

Extended Data Table 1 | Antibodies used in this study

Antibody, anti-	Supplier	Clone	Host	Dilution	Application
Mouse CD3e	BD Pharmingen	145-2C11	Hamster	1:100	Plate/glass coating
Mouse IFNγ	Biolegend	XMG1.2	Rat	1:200	FC, ICC
Mouse IFNγ-Alexa488	Biolegend	XMG1.2	Rat	1:200	FC, ICC
Mouse GzmB-Alexa647	Biolegend	GB11	Rat	1:200	FC, ICC
Mouse-CRTAM-PE	Biolegend	11-5	Rat	1:200	FC
Mouse-CD25-FITC	BD Pharmingen	7D4	Rat	1:200	FC
Mouse-CD44-PE	BD Bioscience	IM7	Rat	1:1200	FC
Mouse-CD62L-APC	BD Bioscience	MEL-14 (RUO)	Rat	1:1600	FC
Cis Golgi	BD Bioscience	GM 130	Mouse	1:100	ICC
Mouse-CD107a-PE	BD Bioscience	(1D4B)	Rat	1:200	FC
Mouse-CD69-APC	Thermo Scientific	H1.2F3	Hamst	1:100	FC
Mouse-IgG-Alexa647	Thermo Scientific	—	Goat	1:1000	ICC
Rat-IgG-Alexa647	Thermo Scientific	—	Chicken	1:800	ICC
Mouse-IgG-Alexa568	Thermo Scientific	—	Goat	1:400	ICC

Note: FC: flow cytometry, ICC: immunocytochemistry.

Extended Data

Extended Data Figure 1 | Dynamic expression profiles of CD44 and CD62L in reactivated CTLs. WT cytotoxic T lymphocytes (CTLs) activated for 3-5 days were re-stimulated with plate-bound anti-CD3e antibody (10 μg/mL) for the indicated durations (0, 0.5, 1, 2, 3, and 4 hours), followed by intracellular staining for IFNγ and granzyme B (GzmB). **(A, C)** Fold change in the percentage of CD44+ and CD62L+ cells. (**B,D)** Median fluorescence intensity (MFI) of CD44-PE (rat anti-mouse) and CD62L-APC (rat anti-mouse). Data represent mean ± SEM from ≥3 independent experiments. Statistical significance was determined by one-way ANOVA with post hoc unpaired t-tests: NS, $p > 0.05$; *$0.01 < p \leq 0.05$; **$0.001 < p \leq 0.01$; ***$0.0001 < p \leq 0.001$.

Extended Data Figure 2 | Flow cytometric analysis of T cell activation markers. WT cytotoxic T lymphocytes (CTLs) activated for 3–5 days were re-stimulated with plate-bound anti-CD3e antibody (10 μg/mL) for 0–4 hours and stained for surface expression of CD44 and CD62L. (**A)** Median fluorescence intensity (MFI) of CD44-PE (rat anti-mouse) in CD44+ IFNγ^{hi} and IFNγ^{lo} CTLs. (**B)** MFI of CD62L-APC (rat anti-mouse) in CD62L+ IFNγ^{hi} and IFNγ^{lo} CTLs. Data represent mean ± SEM from ≥3 independent experiments. Statistical analysis was performed using one-way ANOVA followed by unpaired t-tests: NS, $p > 0.05$; *$0.01 < p \leq 0.05$; **$0.001 < p \leq 0.01$; ***$0.0001 < p \leq 0.001$.

Extended Data Figure 3 | Temporal dynamics of IFNγ and granzyme B expression in activated CTLs. WT cytotoxic T lymphocytes (CTLs) activated for 4 days were re-stimulated with plate-bound anti-CD3e monoclonal antibody (10 μg/mL) for 4–24 hours. Cells were subsequently stained for intracellular IFNγ and GzmB using fluorescently labeled antibodies and analyzed by flow cytometry (FlowJo v10.10.0). (**A)** IFNγ fluorescence intensity changes in IFNγ^{hi} and IFNγ^{lo} subsets. (**B)** GzmB fluorescence intensity changes in IFNγ^{hi} and IFNγ^{lo} subsets. Data represent mean ± SEM from 3 independent experiments. Statistical significance was determined by one-way ANOVA followed by unpaired t-tests: NS, $p > 0.05$, *$0.01 < p \leq 0.05$, **$0.001 < p \leq 0.01$, ***$0.0001 < p \leq 0.001$.

Extended Data Figure 4 | Temporal profiling of activation markers and IFNγ expression in primary CTLs. Day 0 WT cytotoxic T lymphocytes (CTLs) were stimulated in 96-well plates with plate-bound anti-CD3e (10 μg/mL) and anti-CD28 (5 μg/mL) antibodies for 0 h, 3 h, 6 h, 14 h, 24 h, 48 h,and 72 h , followed by surface staining for CRTAM, CD62L, CD69, and CD25, and intracellular staining for IFNγ. **(A)** Pseudocolor plots showing temporal expression patterns of CRTAM and IFNγ in day 0 CTLs following stimulation. (**D, G, J)** Pseudocolor plots depicting dynamic expression of CD62L, CD69, and CD25 in day 0 CTLs. **(B, E, H, K)** Quantification of CRTAM+, IFNγ+, CD62L+, CD69+, and CD25+ cell populations in stimulated day 0 CTLs. **(C, F, I, L)** Quantification of CRTAM-PE, IFNγ-Alexa488, CD62L-APC, CD69-APC, and CD25-PE median fluorescence intensity. Data represent mean ± SEM.

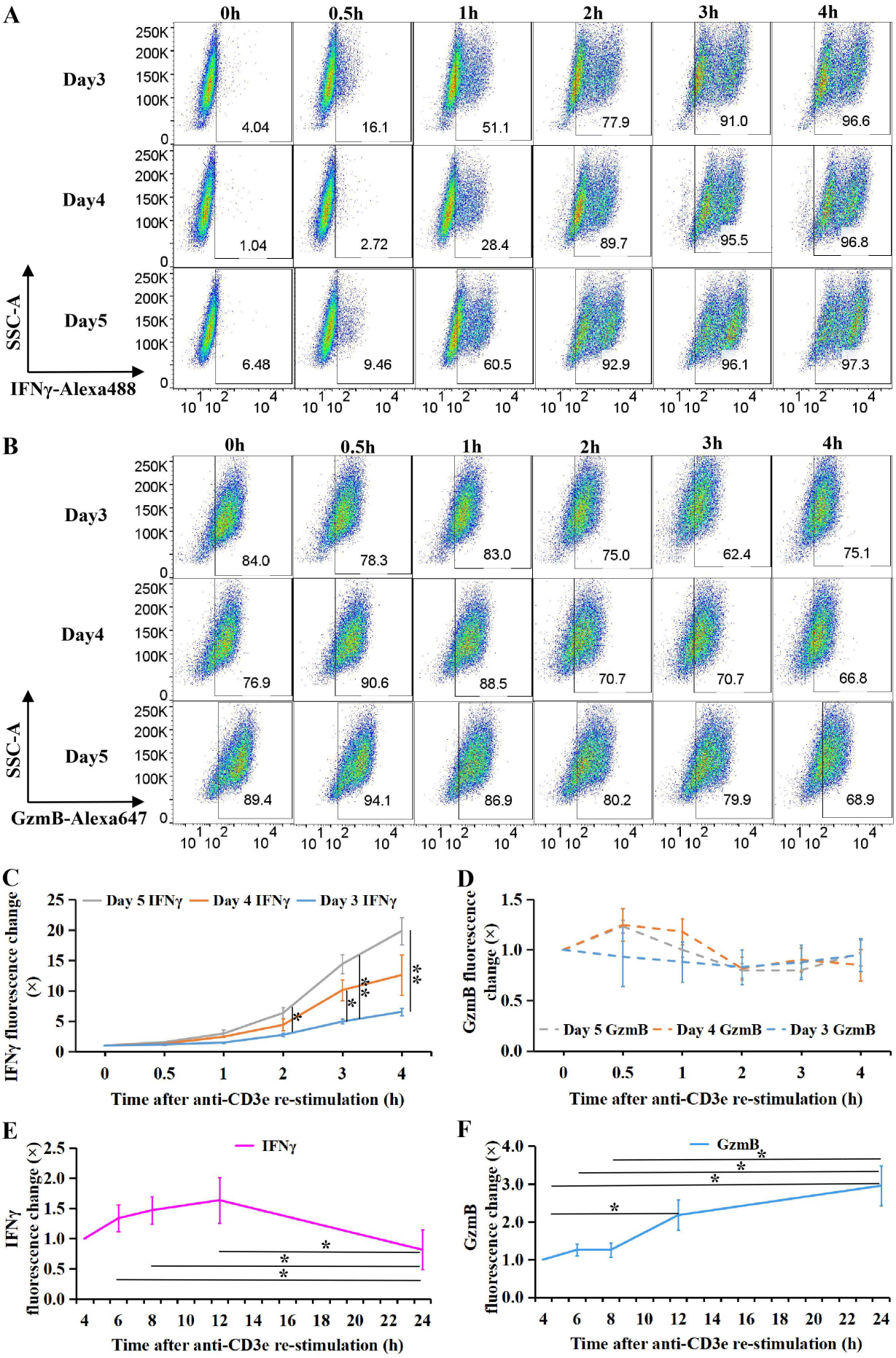
A
0h
0.5h
1h
2h
3h
4h
Day3
Day4
Day5
SSC-A
IFNγ-Alexa488
4.04
16.1
51.1
77.9
91.0
96.6
1.04
2.72
28.4
89.7
95.5
96.8
6.48
9.46
60.5
92.9
96.1
97.3
B
GzmB-Alexa647
84.0
78.3
83.0
75.0
62.4
75.1
76.9
90.6
88.5
70.7
70.7
66.8
89.4
94.1
86.9
80.2
79.9
68.9
C
IFNγ fluorescence change (×)
Day 5 IFNγ
Day 4 IFNγ
Day 3 IFNγ
Time after anti-CD3e re-stimulation (h)
D
GzmB fluorescence change (×)
Day 5 GzmB
Day 4 GzmB
Day 3 GzmB
Time after anti-CD3e re-stimulation (h)
E
IFNγ fluorescence change (×)
IFNγ
Time after anti-CD3e re-stimulation (h)
F
GzmB fluorescence change (×)
GzmB
Time after anti-CD3e re-stimulation (h)

Figure 1

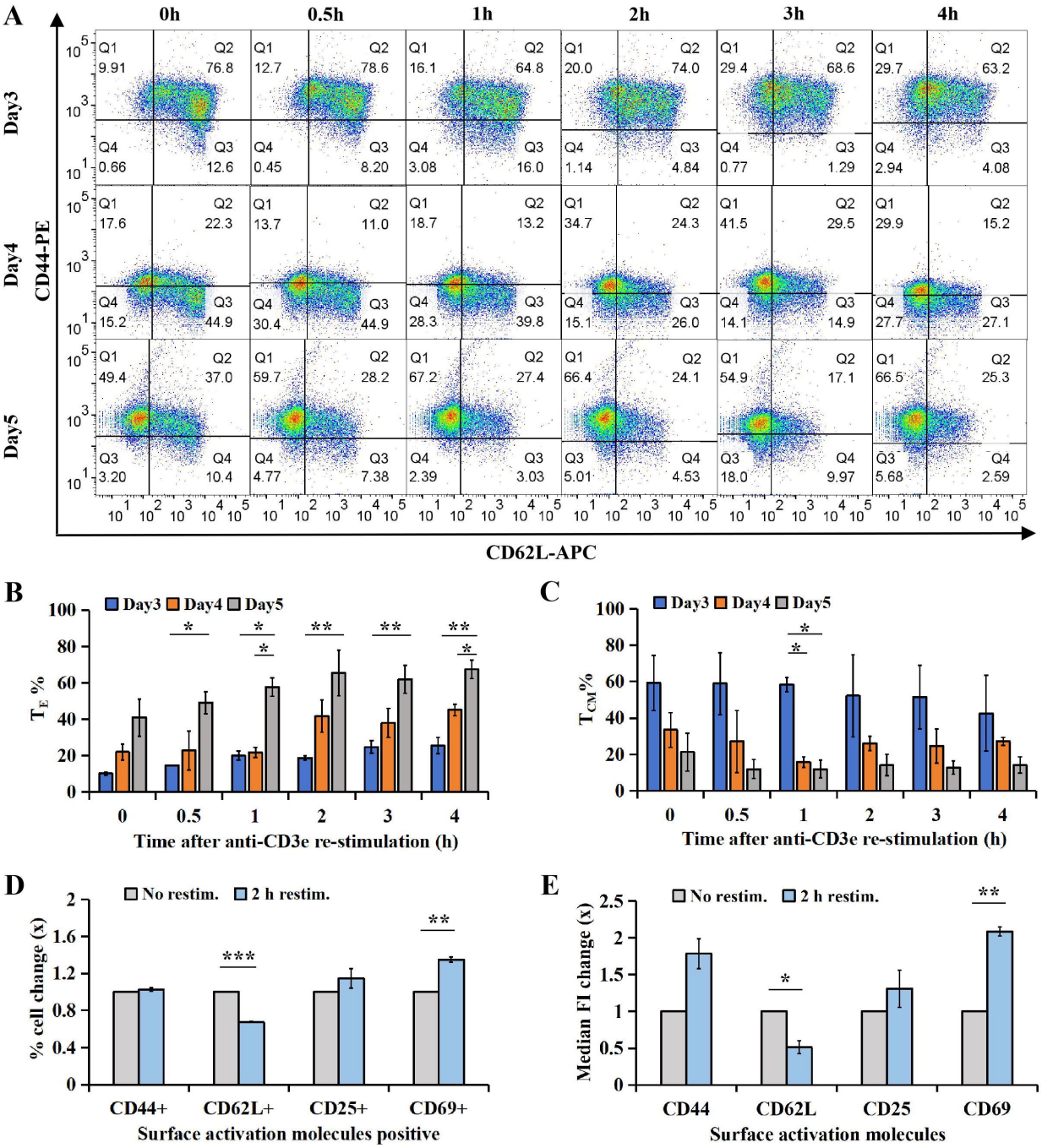
A
0h
0.5h
1h
2h
3h
4h
Day3
Day4
Day5
CD44-PE
CD62L-APC
B
Day3 Day4 Day5
T_E %
Time after anti-CD3e re-stimulation (h)
C
Day3 Day4 Day5
T_{CM} %
Time after anti-CD3e re-stimulation (h)
D
No restim. 2 h restim.
% cell change (x)
CD44+ CD62L+ CD25+ CD69+
Surface activation molecules positive
E
No restim. 2 h restim.
Median FI change (x)
CD44 CD62L CD25 CD69
Surface activation molecules

Figure 2

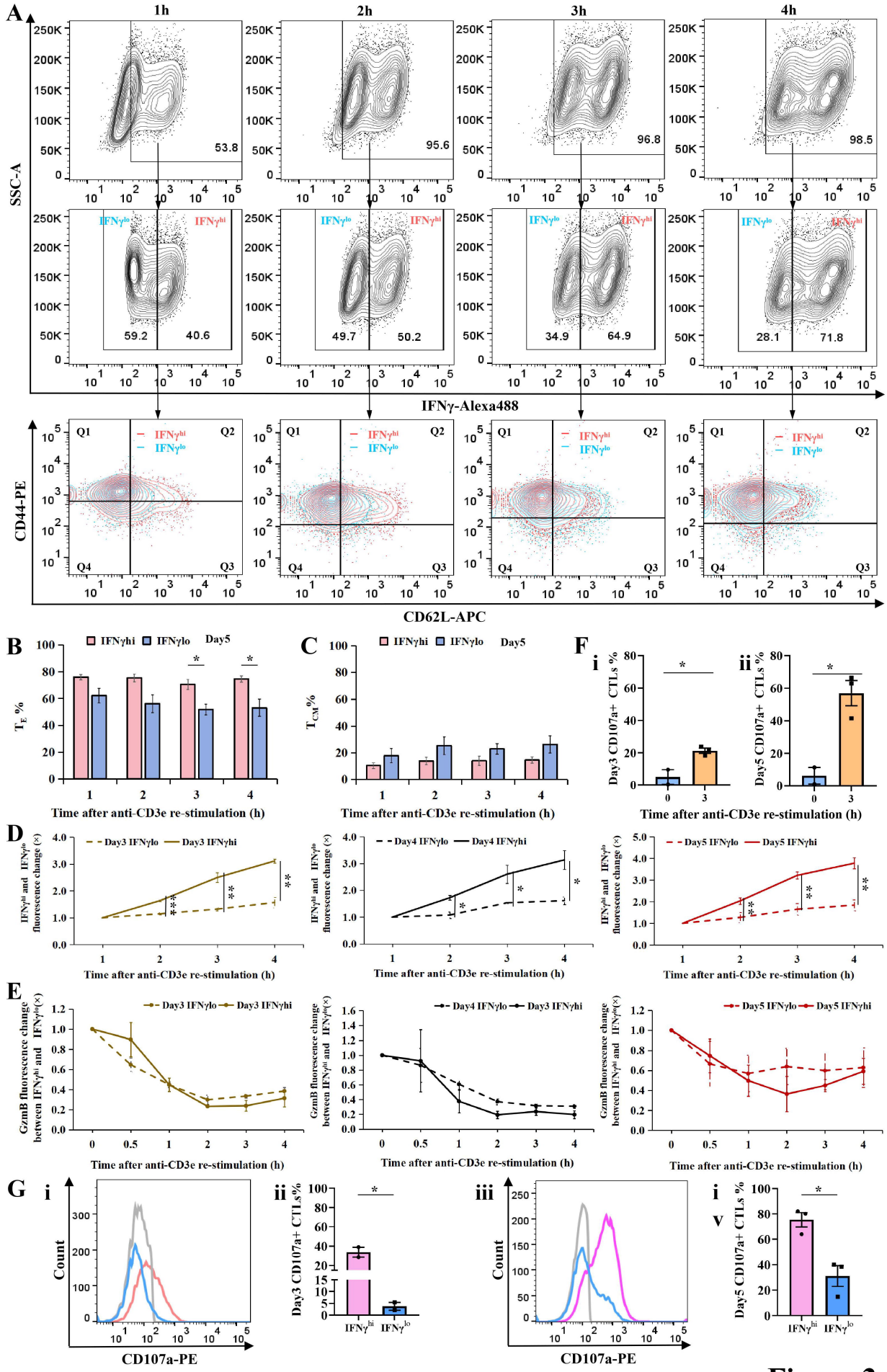
A
1h
2h
3h
4h
SSC-A
53.8
95.6
96.8
98.5
IFNγlo
IFNγhi
59.2
40.6
49.7
50.2
34.9
64.9
28.1
71.8
IFNγ-Alexa488
Q1
Q2
Q3
Q4
CD44-PE
CD62L-APC
B
IFNγhi
IFNγlo
Day5
T_E %
Time after anti-CD3e re-stimulation (h)
C
T_CM %
F
i
ii
Day3 CD107a+ CTLs %
Day5 CD107a+ CTLs %
D
Day3 IFNγlo
Day3 IFNγhi
Day4 IFNγlo
Day4 IFNγhi
Day5 IFNγlo
Day5 IFNγhi
IFNγhi and IFNγlo fluorescence change (×)
E
GzmB fluorescence change between IFNγhi and IFNγlo(×)
G
i
ii
iii
iv
Count
CD107a-PE
Day3 CD107a+ CTLs%
Day5 CD107a+ CTLs %
IFNγhi
IFNγlo

Figure 3

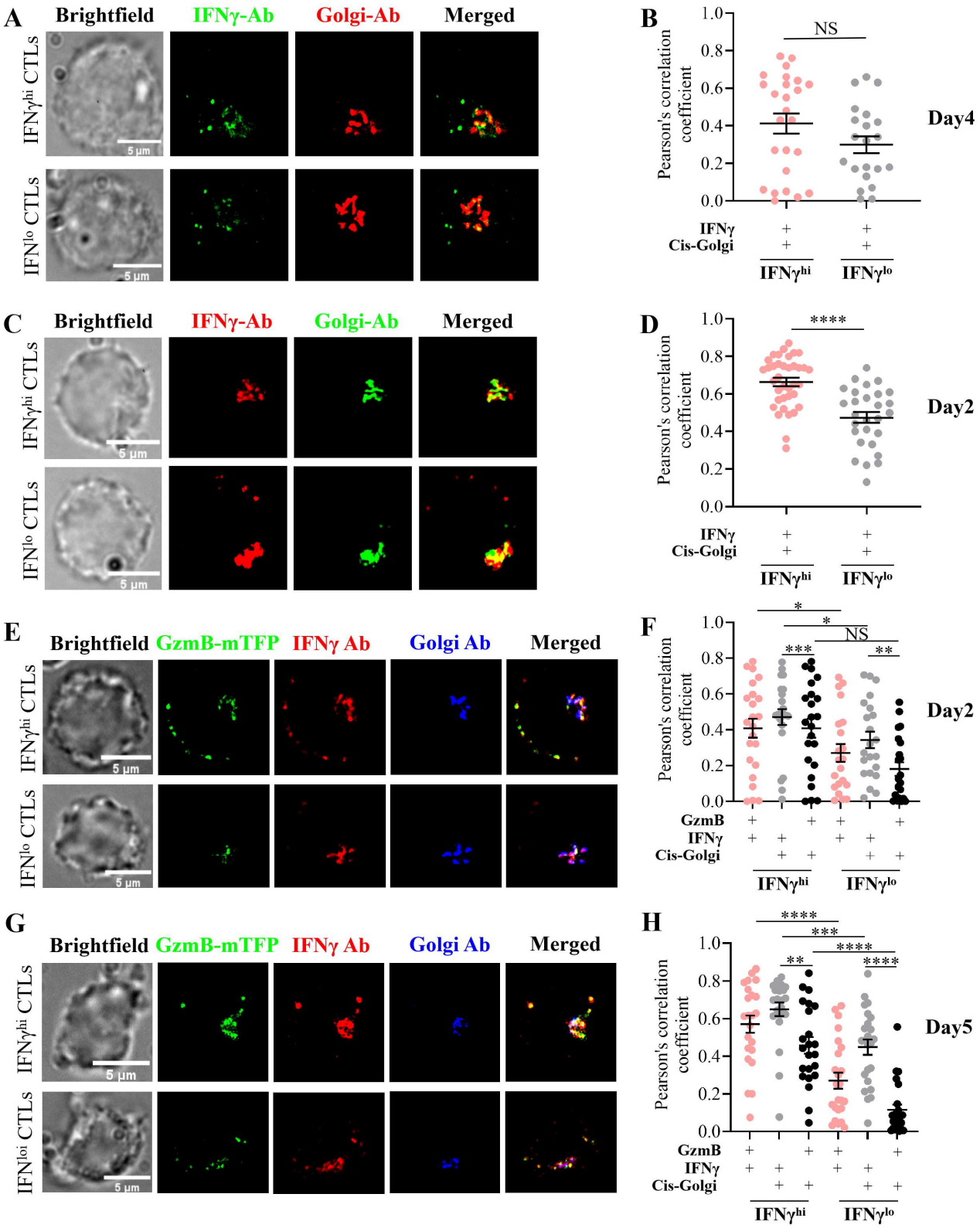
A
Brightfield
IFNγ-Ab
Golgi-Ab
Merged
IFNγhi CTLs
IFNlo CTLs
5 µm
B
Pearson's correlation coefficient
NS
Day4
IFNγ
Cis-Golgi
IFNγhi
IFNγlo
C
D
****
Day2
E
GzmB-mTFP
IFNγ Ab
Golgi Ab
F
*
NS
***
**
GzmB
G
IFNγloi CTLs
H
Day5

Figure 4

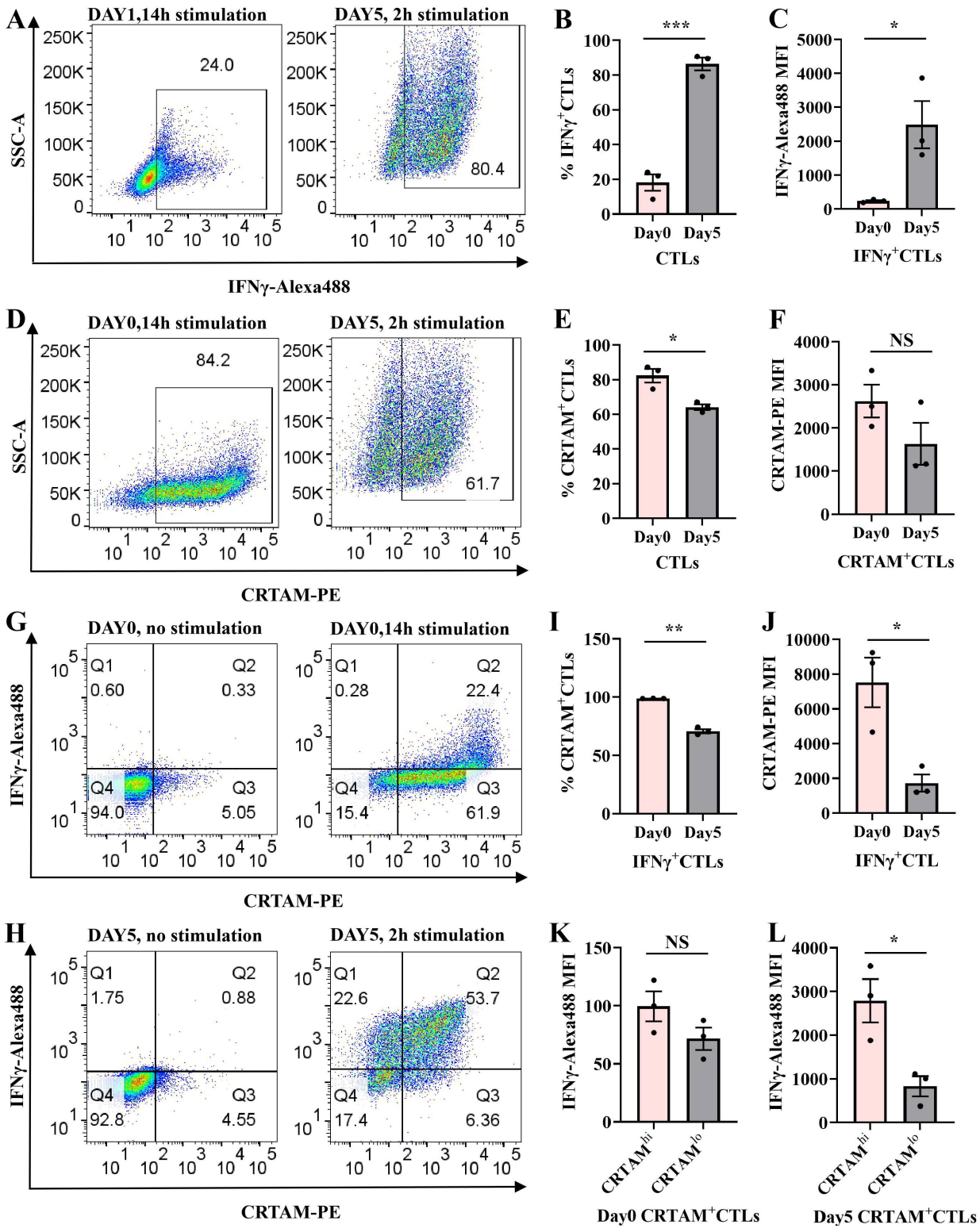
A
DAY1,14h stimulation
DAY5, 2h stimulation
SSC-A
24.0
80.4
IFNγ-Alexa488
B
% IFNγ+CTLs
***
Day0
Day5
CTLs
C
IFNγ-Alexa488 MFI
*
Day0
Day5
IFNγ+CTLs
D
DAY0,14h stimulation
DAY5, 2h stimulation
SSC-A
84.2
61.7
CRTAM-PE
E
% CRTAM+CTLs
*
Day0
Day5
CTLs
F
CRTAM-PE MFI
NS
Day0
Day5
CRTAM+CTLs
G
DAY0, no stimulation
DAY0,14h stimulation
IFNγ-Alexa488
Q1
0.60
Q2
0.33
Q4
94.0
Q3
5.05
Q1
0.28
Q2
22.4
Q4
15.4
Q3
61.9
CRTAM-PE
I
% CRTAM+CTLs
**
Day0
Day5
IFNγ+CTLs
J
CRTAM-PE MFI
*
Day0
Day5
IFNγ+CTL
H
DAY5, no stimulation
DAY5, 2h stimulation
IFNγ-Alexa488
Q1
1.75
Q2
0.88
Q4
92.8
Q3
4.55
Q1
22.6
Q2
53.7
Q4
17.4
Q3
6.36
CRTAM-PE
K
IFNγ-Alexa488 MFI
NS
CRTAMhi
CRTAMlo
Day0 CRTAM+CTLs
L
IFNγ-Alexa488 MFI
*
CRTAMhi
CRTAMlo
Day5 CRTAM+CTLs

Figure 5

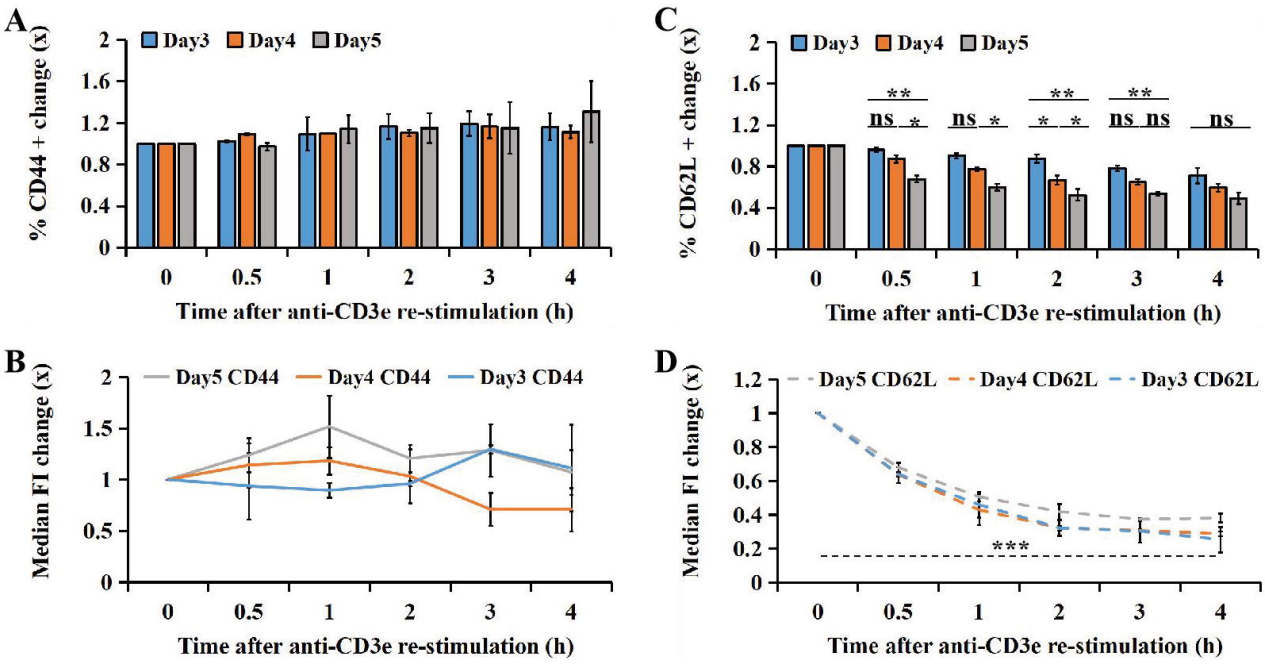

Extended Data Figure 1

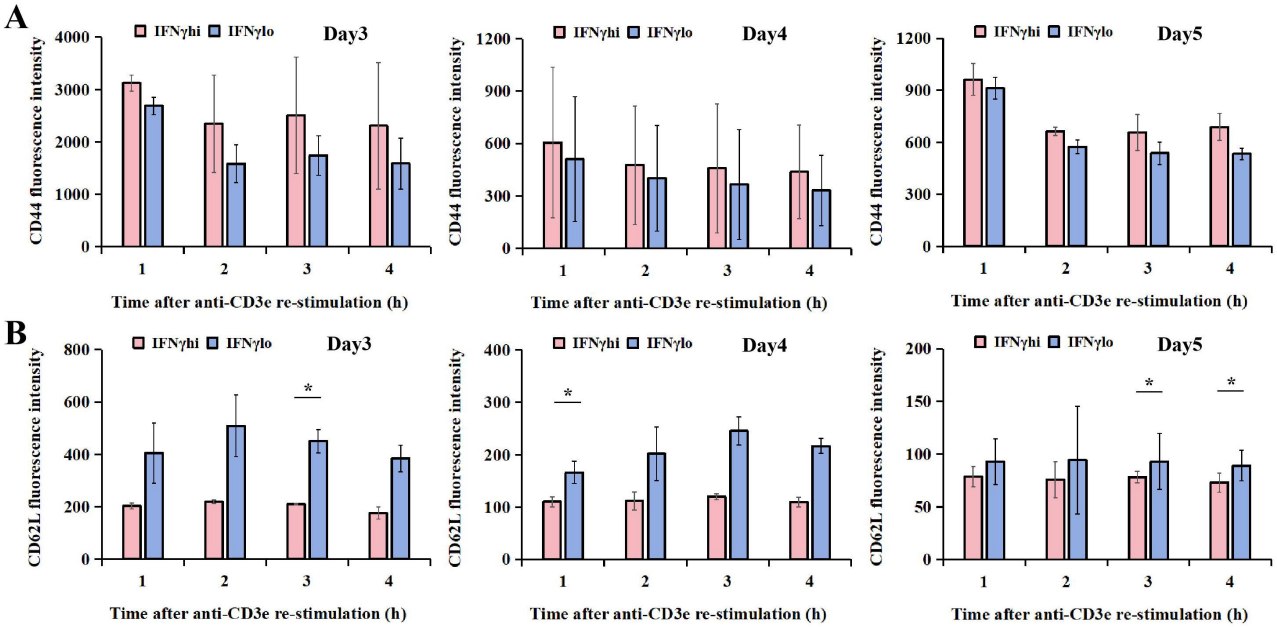

Extended Data Figure 2

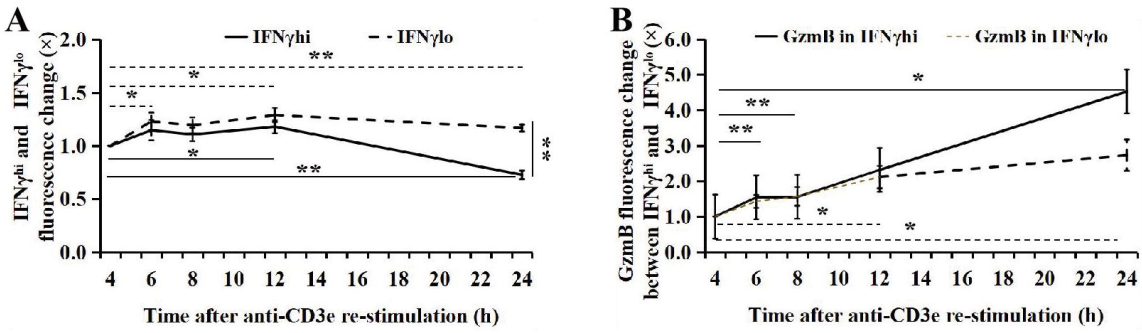

Extended Data Figure 3

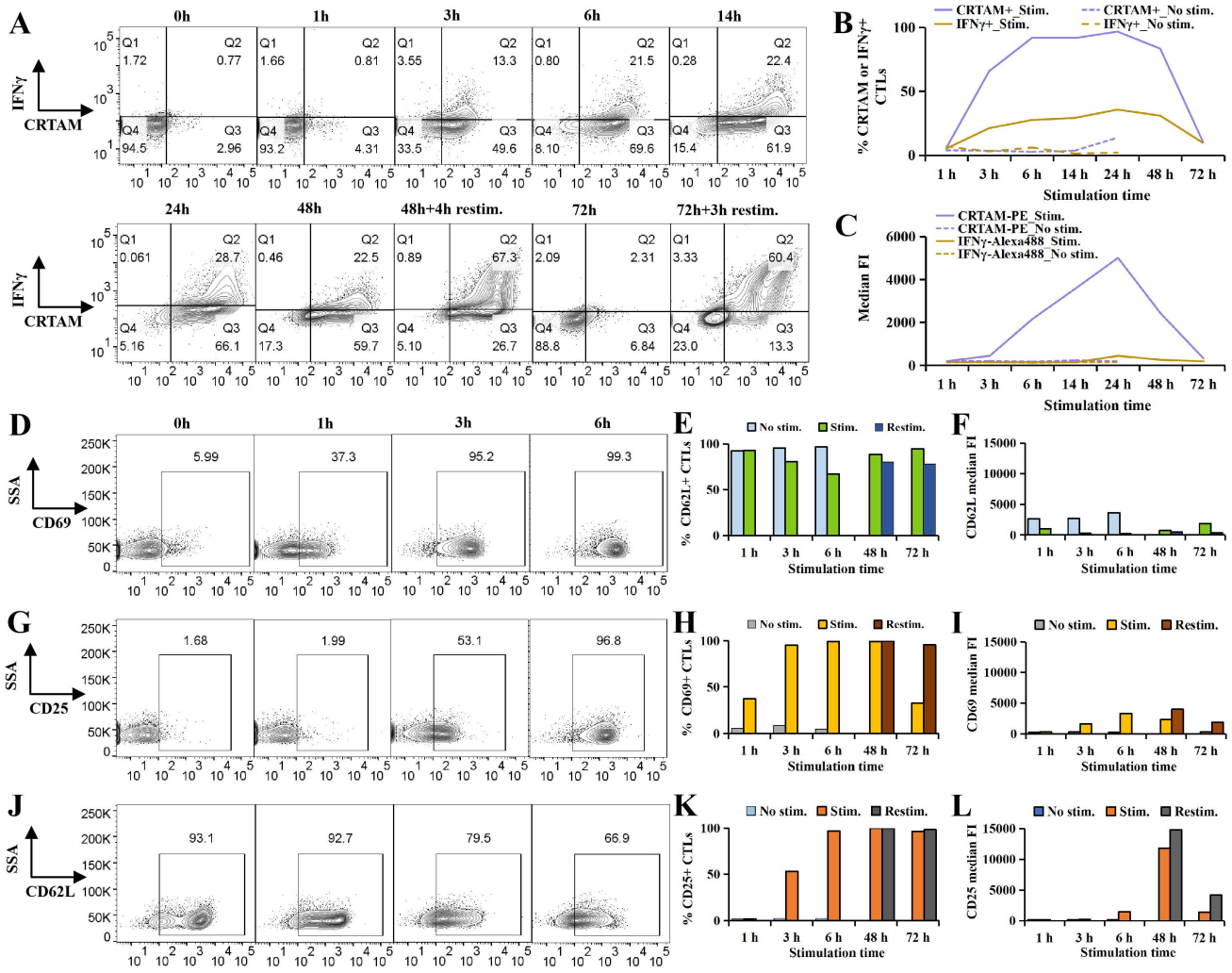

Extended Data Figure 4